Article

Preparation of TiO$_2$-Poly(3-Chloro-2-Hydroxypropyl Methacrylate) Nanocomposite for Selective Adsorption and Degradation of Dyes

M. Shamim Hossan and Bungo Ochiai *

Department of Chemistry and Chemical Engineering, Graduate School of Science and Engineering, Yamagata University, Jonan 4-3-16, Yonezawa, Yamagata 992-8510, Japan; txh01267@st.yagamata-u.ac.jp
* Correspondence: ochiai@yz.yamagata-u.ac.jp; Tel.: +81-238-26-3092

check for updates

Abstract: We report a new nanocomposite TiO$_2$-poly(3-chloro-2-hydroxypropyl methacrylate) (TiO$_2$-PCHPMA) for selective adsorption/degradation of cationic dyes and degradation of anionic dyes. TiO$_2$-PCHPMA was prepared by free radical polymerization of CHPMA in the presence of TiO$_2$ modified with 3-(trimethoxysilyl)propyl methacrylate. TiO$_2$-PCHPMA adsorbed cationic methylene blue (MB), but did not adsorb anionic methyl orange (MO) in their aqueous solutions. The adsorption efficiency for MB reached 99% within 5 min at 28 °C, and adsorbed MB could be recycled in 96% efficiency. The adsorption accelerated degradation of MB under UV irradiation. The degradation of anionic MO proceeded completely with TiO$_2$-PCHPMA under UV irradiation, and the efficiency was not affected by the PCHPMA layer. TiO$_2$-PCHPMA is potentially applicable as a material capable of selective removal and recovery of cationic dyes, and degradation of other dyes from industrial effluents.

Keywords: dye; selectivity; degradation; adsorption; water treatment

1. Introduction

Dyes are extensively used in various industrial processes, and their annual market is more than 7×10^5 t/year [1]. More than 10% of the amounts of dyes are discharged into the environment during industrial process [2]. Specifically, synthetic dyes composed of structures with stable aromatic backbones are not biodegradable, and their polluting nature is of considerable environmental concern [3]. Materials for degradation and removal of such dyes are in high demand.

TiO$_2$ has been widely used as an efficient photocatalyst for degradation of various pollutants due to its high activity associated with the low cost, low toxicity, and high photo- and chemical stability [4–53]. The structure of TiO$_2$ can be tailored by surface modification or doping for enhancement of the performance of TiO$_2$ on photocatalytic activity, availability of pollutant, processability etc. [49,50]. For example, TiO$_2$ has been hybridized or modified with metals [5–7], organic substances including polymers [23–48], and carbon materials [8–10] including carbon nanotubes [11–13], activated carbon [14–16], graphene [17–19], and graphene oxide [20–22]. Such modifications sometimes deteriorate the photocatalytic performance due to prevention of charge transfer. Accordingly, appropriate designs are necessary to develop TiO$_2$ materials with additional properties.

Selectivity is a major drawback of TiO$_2$, but is very important in targeting pollutants in the treatment of waste water, which typically contains high concentration of non-hazardous substances. For selective photocatalytic degradation, the surface structure is the important factor in controlling the selectivity of adsorption. Ionic surfaces on TiO$_2$ enable selective degradation of cationic and anionic

pollutants by interactions with organic pollutants with opposite charges [42,43,50–52]. For example, TiO_2 with positive and negative surface charges fabricated using Na_2CO_3 and NH_4OH is highly active for selective degradation of cationic methylene blue (MB) and anionic methyl orange (MO), respectively, from their aqueous mixture [52]. Molecular imprinting was also employed for selective degradation. TiO_2 coated with thin layers of polymers imprinting 2-nitrophenol and 4-nitrophenol was prepared by polymerization of *o*-phenylenediamine in the presence of TiO_2 nanoparticles and the target molecules. The resulting imprinted TiO_2 composites photodegraded the targets predominantly over other coexisting pollutants [44]. Control of polarity was also used for selective adsorption [45]. Hydrophobic TiO_2 can be prepared by modifying the surface of TiO_2 nanoparticles (P25) with long alkyl chains such as *n*-octyl groups (MS-P25oct). The hydrophobic character of MS-P25oct enabled adsorption of hydrophobic substances, which led to selective degradation of 4-nonylphenol (NLP). Contrary to this TiO_2, a core-shell nanocomposite consisting of P25 and mesoporous silica (CMS-P25) with a more hydrophilic surface was developed for selective degradation of NLP and phenol (PL) from an aqueous mixture of NLP, PL, and nonane, while the mechanism of the selection is unclear [46]. Such selectivity depends on the characters of the functional groups and the spaces to capture target pollutants, and the modification to improve affinity basically assisting selective degradation. Challenges for such modification involve higher selectivity, higher stability, and higher capacity.

In this study, we designed TiO_2-poly (3-chloro-2-hydroxypropyl methacrylate) (TiO_2-PCHPMA) as a photocatalyst for recycling and degradation of dyes with selectivity depending on the ionic character of the dyes. PCHPMA has been employed as a scaffold of modification with various functionalities for selective interactions in aqueous media by the electrostatic interaction of the chloroalkyl moieties and the moderate hydrophilicity of the hydroxy groups [54].

In the course of our study, TiO_2-PCHPMA was synthesized and examined for removal of organophosphorus pesticides for comparison with TiO_2 modified with polystyrene [55]. However, this TiO_2-PCHPMA showed weaker interaction with the examined pesticides than the polystyrene analogue. The pesticides consist of hydrophobic and non-ionic structures, and the similarity with polystyrene resulted in the higher removal efficiency of TiO_2 modified with polystyrene. The utility of PCHPMA depends on the chloroalkyl moieties for selective interactions, namely the electrostatic interactions based on the Lewis-basic chloride group. We targeted electrostatic selection of ionic dyes for separation and degradation. The adsorption and degradation experiments of dyes using TiO_2-PCHPMA were conducted, and revealed that TiO_2-PCHPMA is an efficient material for adsorption of MB and photocatalytic degradation of MO. As a result of selective adsorption, MB could be either recycled or degraded. This clear difference originated from the electrostatic adsorption of MB on the layer of PCHPMA and the moderate hydrophilicity of PCHPMA allowing diffusion of MO around the TiO_2 core.

2. E.xperimental Section

2.1. Materials

Tetra-isopropyl orthotitanate (TIPOT), 3-chloro-2-hydroxypropyl methacrylate (CHPMA), and 3-(trimethoxysilyl)propyl methacrylate (MPS) were purchased from Tokyo Chemical Industry Co., Ltd. (Tokyo, Japan). Dibenzoyl peroxide (BPO), methylene blue (MB), methanol (MeOH), ethanol (EtOH), 1,4-dioxane, acetic acid, and aqueous ammonia solution (28 wt%) were purchased from Kanto Chemical Co., Inc. (Tokyo, Japan). Methyl orange (MO) was purchased from Wako Pure Chemical Industry, Ltd. (Tokyo, Japan). Water was purified with MINIPURI TW-3000RU (Nomura Micro Science Co., Ltd., Kanagawa, Japan). All materials used were analytical grade reagents, and used without further purification.

2.2. Measurements and Instrument

Scanning electron microscopy (SEM) measurements were conducted on a Hitachi SU8000 microscope (Hitachi, Ltd., Tokyo, Japan). Energy-dispersive X-ray (EDX) analysis was carried out on a JEOL JSM-6510A scanning electron microscope (JEOL Ltd., Tokyo, Japan) equipped with a JEOL JED 2300 EDX spectrometer. The samples for EDX were molded as disks and placed on a carbon tape. Transmission electron microscopy (TEM) measurements were carried out on a JEOL TEM-2100F field emission electron microscope. Hydrodynamic size and zeta potential were measured by dynamic light scattering (DLS) analysis conducted on a Malvern Zetasizer Nano ZS instrument (Malvern Instruments, Ltd., Malvern, UK). Fourier transform infrared (FTIR) spectra were measured on a JASCO FT/IR-460 spectrometer (JASCO Co., Tokyo, Japan). Thermogravimetric analysis (TGA) was carried out on a Seiko (Tokyo, Japan) TG/DTA 6200 (EXSTER6000) instrument at a heating rate of 10 °C/min under N_2 atmosphere. A UV visible light (input current 1.35 A, 121 W, frequency 50 Hz) model HLR100T-2 (SEN lights corp., Osaka, Japan) was utilized as the illumination light source. Optical absorbance was measured on a HACH DR 5000 UV visible spectrometer (HACH Com., Loveland, Colorado, USA). Centrifugation was carried out on a Kubota KN-70 centrifugation machine (Kubota Corp., Osaka, Japan). Cyclic voltammetry (CV) measurements were carried out on an ECstat-301 potentio/galvnostat analyzer (EC Frontier, Kyoto, Japan). The working electrodes were prepared by drying a Pt electrode dipped into 0.1 g/L THF solutions of the samples. Ag and Pt were employed as the reference and counter electrodes, respectively. Supporting electrolyte was 0.1 M NaCl solution.

2.3. Preparation of TiO$_2$ Nanoparticles from TIPOT

TIPOT (7.68 g, 2.70×10^{-2} mol) was dispersed in 20 mL of EtOH with magnetic stirring for 20 min. Then, a mixture of acetic acid (1.2 mL) and deionized water (250 mL) was added to the dispersion under vigorous magnetic stirring, and the reaction was continued for 20 h at 60 °C. After the reaction, the product was collected by centrifugation and washed with EtOH. This centrifugation–dispersion washing process was repeated 5 times. TiO$_2$ nanoparticles were obtained by drying at 60 °C for 24 h under vacuum (2.12 g, 2.65×10^{-2} mol, 98.2% yield).

2.4. Preparation of TiO$_2$-MPS

TiO$_2$ (2.02 g) was dispersed in EtOH (50 mL) by ultrasonication for 30 min. Then, deionized water (1.25 g), NH$_3$ solution (0.62 g), and MPS (1.11 g, 2.32×10^{-4} mol) were added to the dispersion. The mixture was magnetically stirred for 24 h at 60 °C under a nitrogen atmosphere. The product was collected after 5 times of centrifugation–dispersion with EtOH. TiO$_2$-MPS was obtained by drying at 60 °C for 24 h under vacuum (1.82 g, 58.1% yield).

2.5. Preparation of TiO$_2$-PCHPMA

TiO$_2$-MPS (1.53 g) was dispersed in 1,4-dioxane (20 mL) in a round-bottomed flask immersed in a thermostat oil bath maintained at 70° C. CHPMA (3.10 g, 3.47×10^{-4} mol) and BPO (15 mg, 1.2×10^{-6} mol) were added to the flask. The free radical polymerization was conducted at 70 °C for 24 h under a nitrogen atmosphere. The product was washed 5 times with centrifugation–dispersion in EtOH. TiO$_2$-PCHPMA was obtained by drying at 60 °C for 24 h under vacuum as a yellowish solid (1.31 g, 28.3% yield).

2.6. Adsorption Experiment

The solutions of MB and MO (10 mg/L) were prepared by dissolving in purified water. Experiments on the adsorption of these dyes were carried out using 8 mg of adsorbents TiO$_2$-PCHPMA or PCHPMA for 10 mL of the MB and MO solutions at 28 °C in an AS ONE I-cover incubator installed with a magnetic stirrer. The mixture was centrifuged at 5000 rpm for 15 min after a desired time interval. The dyes adsorbed were eluted with MeOH 3 times by the centrifugation–dispersion process.

The elutant was concentrated by evaporating MeOH with a BÜCHI R-205 Rotavapor (Nihon Büchi Co., Tokyo, Japan), and the elutant with adjusted volume was subjected to UV-visible measurement. The final concentrations of MB and MO in the supernatants after the adsorption were also measured by UV-visible measurements. The concentrations were calculated based on the calibration curves of MB and MO.

The adsorption ratio (r_{ad} in %) and the amount of adsorbed dyes (q_t in mg/g) on TiO$_2$-PCHPMA in a certain time interval were calculated from the following Equations (1) and (2), respectively;

$$r_{ad} = \frac{c_0 - c_t}{c_0} \times 100 \tag{1}$$

$$q_t = \frac{c_0 - c_t}{m} \times v \tag{2}$$

where c_0 (mg/L) is the initial concentration; c_t (mg/L) is the residual concentration of cationic dyes at time t in liquid phase after adsorption; v (L) is the volume of solution of dyes; and m (g) is the weight of the adsorbent.

Adsorption experiments under varied pH conditions were carried out by adjusting the pH with 0.1 M HCl and 0.1 M NaOH aqueous solutions.

2.7. Degradation Experiment

The aqueous solutions of MO and MB (10 mg/L) were mixed with TiO$_2$ or TiO$_2$-PCHPMA (0.40 mg/mL) in Pyrex glass beakers with magnetic stirring for 20 min in dark conditions. Then, the suspensions were UV-irradiated for the desired time. After the UV irradiation, the suspension was centrifuged for 15 min at 5000 rpm. The supernatant was decanted, and the volume was adjusted with water for UV-visible measurements. The precipitate was washed 3 times with the centrifugation–dispersion process with hot water (45 °C) for MO, and MeOH for MB to elute the dyes. The elutants were concentrated with a BÜCHI R-205 Rotavapor, and the elutants with adjusted volume were subjected to UV-visible measurement.

The degradation ratio of MO and MB in the presence of TiO$_2$-PCHPMA in a certain time (r_{deg} in %) was calculated from the following Equation (3);

$$r_{deg} = \frac{a_0 - a_t}{a_0} \times 100 \tag{3}$$

where a_0 is the absorbance of initial dye concentration and a_t is the absorbance of dye in the liquid phase after degradation at time t.
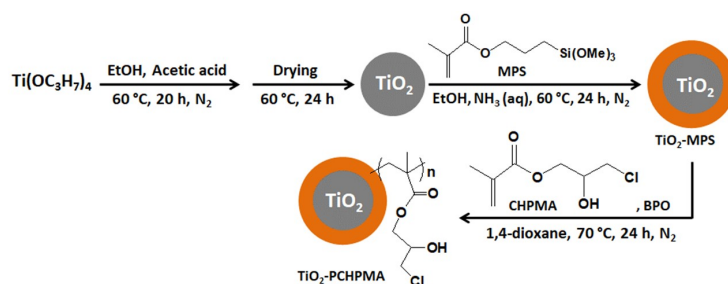

Figure 1. Scheme for the preparation of TiO$_2$-poly(3-chloro-2-hydroxypropyl methacrylate) (TiO$_2$-PCHPMA).

3. Results and Discussion

3.1. Characterization

TiO$_2$-PCHPMA was prepared by sequential reactions of condensation of TIPOT, coating with MPS, and radical polymerization of CHPMA in the presence of TiO$_2$-MPS (Figure 1). The morphology of TiO$_2$, TiO$_2$-MPS, and TiO$_2$-PCHPMA was observed by SEM (Figure 2a–c). The particles were agglomerated and non-uniform in shape. The ranges of the sizes of the primary particles of TiO$_2$, TiO$_2$-MPS, and TiO$_2$-PCHPMA were approximately 15–45 nm, 20–60 nm, and 22–90 nm, respectively. The gradual increase in size is attributed to the formation of the MPS and PCHPMA layers on the TiO$_2$ surface. The morphology was also changed after the surface modifications of TiO$_2$ with MPS and PCHPMA. The particles of TiO$_2$ were simply aggregated and showed their bare surface. By contrast, TiO$_2$-MPS and TiO$_2$-PCHPMA were fused, and the interfaces unclear due to the organic components serving as glue. This tendency was more significant in the image of TiO$_2$-PCHPMA having a higher content of organic component. The morphology of TiO$_2$, TiO$_2$-MPS, and TiO$_2$-PCHPMA was also observed by TEM (Figure 2d–f). The TEM image of TiO$_2$-PCHPMA shows the size of the primary particles in the range of 1–8 nm, which is significantly smaller than that in the SEM image. This image shows grains with sizes identical to those observed in the SEM image consisting of agglomerated primary particles. This difference indicates that the grains were grown by the fusion of nanoparticles. The TEM images of TiO$_2$-MPS and TiO$_2$-PCHPMA also show grains consisting of aggregated nanoparticles, while the grains are not fused. The organic layers probably reduced the interparticle interactions, and improved the dispersibility.
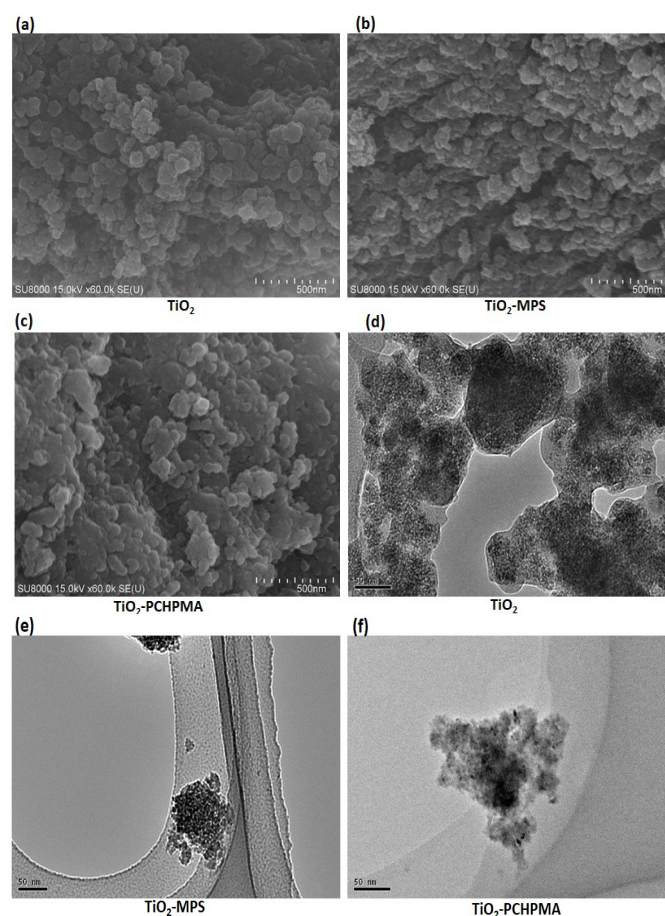

Figure 2. Scanning electron microscopy (SEM) images of (**a**) TiO$_2$, (**b**) TiO$_2$-MPS, and (**c**) TiO$_2$-PCHPMA (scale bar = 500 nm); and transmission electron microscopy (TEM) images of (**d**) TiO$_2$, (**e**) TiO$_2$-MPS, and (**f**) TiO$_2$-PCHPMA (scale bar = 50 nm).

The formation of TiO$_2$-PCHPMA was confirmed by EDX, FTIR, and TGA analyses. Figure 3a indicates the EDX spectra of TiO$_2$, TiO$_2$-MPS, and TiO$_2$-PCHPMA for evaluation of the elemental compositions. The EDX spectrum of TiO$_2$ exhibited major peaks originating from Ti and O. A minor peak of C is attributable to the organic residue of TIPOT and the carbon tape substrate. The EDX spectrum of TiO$_2$-MPS shows a new peak of Si, indicating the successful modification of TiO$_2$ with MPS. The EDX spectrum of TiO$_2$-PCHPMA shows another new peak of Cl. The relative intensities of the peaks of C and O compared to the peak of Ti are larger than those of TiO$_2$, supporting the increase of the organic component originating from the PCHPMA layer.

The structure of TiO$_2$-PCHPMA was evaluated by FTIR spectroscopy (Figure 3b). Broad absorption peaks originating from the Ti–O bond were observed around 620 cm^{-1} in the FTIR spectra of unmodified TiO$_2$, TiO$_2$-MPS, and TiO$_2$-PCHPMA [56]. The spectrum of the precursor TiO$_2$-MPS showed characteristic peaks originating from MPS at 2986, 1717, 1680, 1461, 1192, and 1042 cm^{-1}, assigned to the C–H, C=O, and C=C stretching, C–H bending, C–O–C and Ti–O–Si stretching vibrations, respectively [47,57,58]. The FTIR spectrum of TiO$_2$-PCHPMA exhibits a weak absorption peak around 750 cm^{-1} assignable to the C–Cl bonds as observed in the spectrum of PCHPMA. The absorption peaks at 1740 and 1196 cm^{-1} are assignable to the characteristic stretching vibration of the C=O and C–O bonds in the ester group in the PCHPMA structure. As a result of the grafting of PCHPMA, the FTIR spectrum of TiO$_2$-PCHPMA shows an absorption of the C–H stretching vibration at 2987 cm^{-1} with a higher relative intensity and the absorption peaks at 1170 and 620 cm^{-1} of the Ti–O–Si and Ti–O bonds with weaker relative intensities than the spectrum of TiO$_2$-MPS.
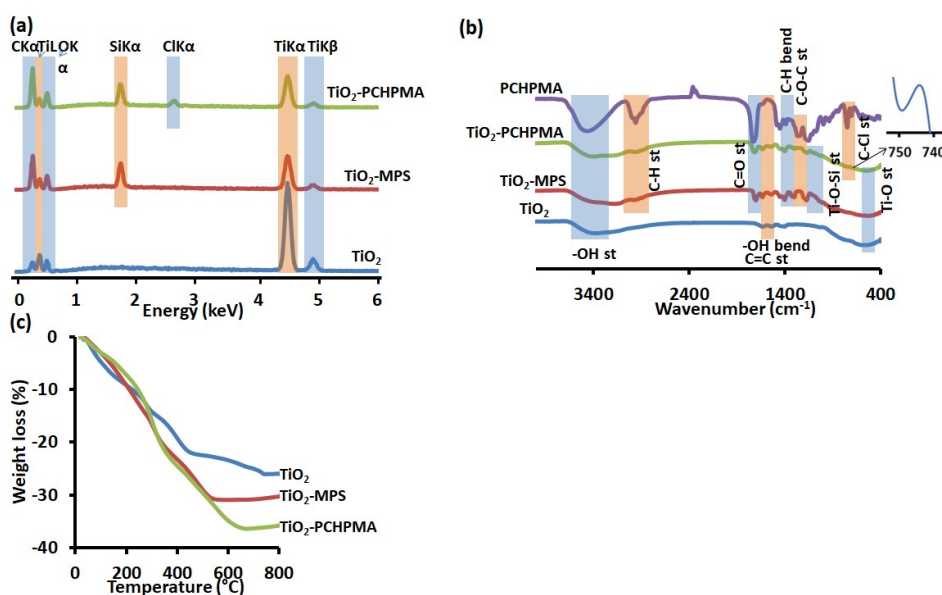
Figure 3. (**a**) Energy-dispersive X-ray (EDX) spectra, (**b**) Fourier transform infrared (FTIR) spectra, and (**c**) thermogravimetric analysis (TGA) curves (10 °C/min, N$_2$) of TiO$_2$, TiO$_2$-MPS, and TiO$_2$-PCHPMA.

The compositions of the organic structures were estimated by TGA (Figure 3c). The TGA curve of TiO$_2$-PCHPMA exhibited three-stage weight loss as observed for various TiO$_2$-polymer composites [11,20,48,57,58]. The first approximately 10% weight loss below 200 °C originates from the evaporation of physiosorbed water and alcohols on the nanocomposite surface. The second weight loss took place of approximately 10% at 200–450 °C correlated mainly with the degradation of the organic components [59–61]. The third weight loss occurring above 450 °C is attributed to the loss of water produced by the condensation of neighboring terminal hydroxyl groups of TiO$_2$ [62,63]. The initial weight losses of the modified TiO$_2$ are slower than that of bare TiO$_2$ probably due to the modification of the organic moieties being more hydrophobic than TiO$_2$, but the weight loss became faster after 300 °C due to the degradation of the introduced organic moieties. The TGA profile of TiO$_2$-PCHPMA

shows a more significant effect of the organic component on the slower weight loss at the earlier stage and the faster weight loss at the later stage. The final weight loss of TiO$_2$-PCHPMA reached 36% and the 10% difference from that of TiO$_2$ is comparable to the weight fraction of the organic component.

The SEM, TEM, EDX, FTIR, and TGA analyses confirmed the successful fabrication of TiO$_2$-PCHPMA.
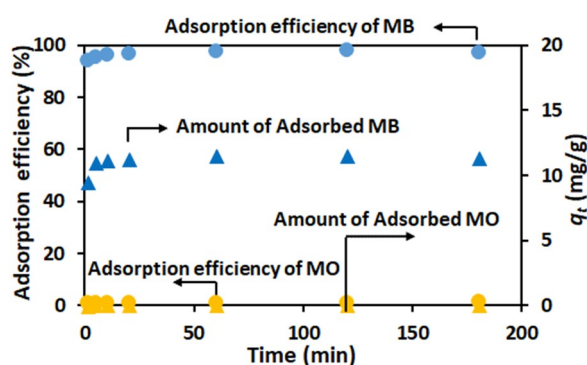
3.2. Adsorption of Dyes

The ability of TiO$_2$-PCHPMA for adsorption and degradation of dyes was evaluated using cationic MB and anionic MO. First, adsorption experiments were conducted for MB and MO at 28 C, and the initial pH values of 5.5 and 6.5, respectively (Figure 4). MB was rapidly adsorbed on TiO$_2$-PCHPMA, while MO was negligibly adsorbed. This tendency is identical to those of both bare TiO$_2$ [42] and PCHPMA. PCHPMA adsorbs MB (3 mg/g-PCHPMA) more efficiently than MO (0.1<mg/g-PCHPMA) by the electrostatic interaction between the Lewis-basic chloride groups in the PCHPMA skeleton and the Lewis-acidic moieties in MB (data not shown). The lower adsorption capacity of PCHPMA is ascribable to the smaller surface area of PCHPMA. The combination of TiO$_2$ and PCHPMA synergistically improved the performance for the adsorption of MB.

This adsorption behavior was investigated by measurement of the zeta potentials of TiO$_2$ and TiO$_2$-PCHPMA before and after adsorption of MB (Table 1). Methanol was used as the medium, as the insufficient dispersibility of the materials in water resulted in unreproducible data. The zeta potential of TiO$_2$-PCHPMA is more negative than that of TiO$_2$, implying a more negative surface suitable for adsorption of cationic MB. The zeta potentials of both TiO$_2$ and TiO$_2$-PCHPMA after adsorption of MB decreased in the negative values, indicating the electrostatic adsorption of cationic MB on the adsorbents. The larger change in the zeta potential of TiO$_2$-PCHPMA clearly supports the higher adsorption capacity originating from the PCHPMA layer.

Table 1. Zeta potentials of TiO$_2$ and TiO$_2$-poly(3-chloro-2-hydroxypropyl methacrylate) (TiO$_2$-PCHPMA)in MeOH before and after adsorption of methylene blue (MB).

| Composites	TiO$_2$		TiO$_2$-PCHPMA	
	Before Adsorption	**After Adsorption**	**Before Adsorption**	**After Adsorption**
Zeta potential (mV)	−9	−7	−26	−10

Figure 4. Time dependence of adsorption efficiency (circle) and relative adsorbed amount (triangle) of MB (blue) and MO (yellow) on TiO$_2$-PCHPMA at 28 °C (concentrations: MB and MO = 10 mg/L, TiO$_2$-PCHPMA = 0.8 mg/mL).

3.3. Effect of pH on the Adsorption of Dyes onto TiO$_2$-PCHPMA

The adsorption experiment was carried out at pH varied from 2 to 13 (Figure 5). The adsorption efficiency for MB exceeded 90% in a wide pH range from 5–12. Below pH 5, the adsorption efficiency of MB was lower probably due to the competition of protonated species such as H$_3$O$^+$ with the cationic

structure of MB. The adsorption efficiency of MB under basic conditions (pH > 12) was lower probably owing to the electrostatic interaction between bases and MB. Additionally, the adsorption efficiencies of anionic MO onto TiO_2-PCHPMA were constantly low above pH 4, indicating the selectivity of the absorption. The adsorption efficiency at pH 3 was higher, probably because MO having a pK_a value of 3.5 is protonated under this acidic condition. The decrease at pH 2 is attributable to the competition with other protonated species in the same manner with MB.

The adsorption ability of TiO_2-PCHPMA was compared with those of other composites of TiO_2 in literatures reporting adsorption and degradation of MB and MO (Table 2). The adsorption ability of TiO_2-PCHPMA toward MB is higher than reported ones. The negligible adsorption of MO indicates the high selectivity of TiO_2-PCHPMA.
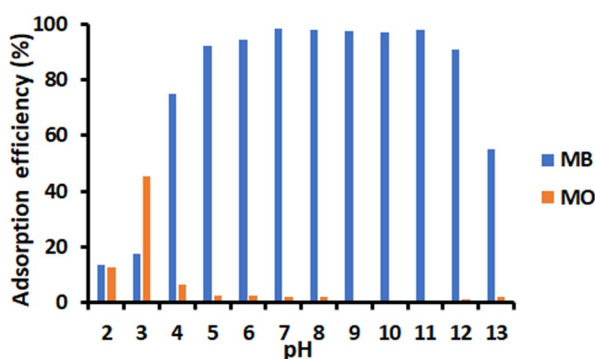
Figure 5. Effect of pH on the adsorption of methylene blue (MB) and methyl orange (MO) by TiO_2-PCHPMA at 28 °C (conditions: dyes = 10 mg/L, TiO_2-PCHPMA = 0.8 mg/mL, 20 min).

Table 2. Adsorption/degradation efficiencies of methylene blue (MB) and methyl orange (MO) by TiO_2 based hybrid composites.

Catalysts	Dye	Adsorption		Degradation		References
		Conditions: concentration of dye (mg/L), composite (g/L) and adsorption time (min)	Efficiency (%)	Conditions: UV irradiation time (min)	Efficiency (%)	
TiO_2/poly[acrylamide-*co*-(acrylic acid)]	MB	5, 0.2, and 15	87	40	91	[40]
TiO_2 treated with Na_2CO_3	MO	10, 1, and 30	23	120	> 99	[52]
TiO_2 treated with NH_4OH	MB	10, 1, and 30	96	60	> 99	
TiO_2-PCHPMA	**MB**	**10, 0.8, and 20**	**99**	**180**	**94**	**This work**
	MO	**10, 0.8, and 20**	**1<**	**180**	**>99**	

3.4. Desorption of MB

MB adsorbed on TiO_2-PCHPMA was washed out with MeOH with 3 times of the centrifugation–dispersion process (Figure 6). MB was quantitively adsorbed on TiO_2-PCHPMA as confirmed by the absence of the absorption of MB in the supernatant. Adsorbed MB was recovered by washing in a desorption efficiency of 96%, indicating that MB was degraded negligibly during the adsorption–desorption process. The slight loss of MB probably originated from the trace degradation, loss of very tiny nanoparticles adsorbing MB not precipitated by the centrifugation, and remaining MB on TiO_2-PCHPMA by the strong adsorption.
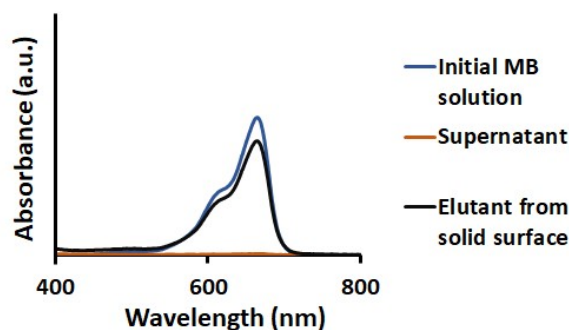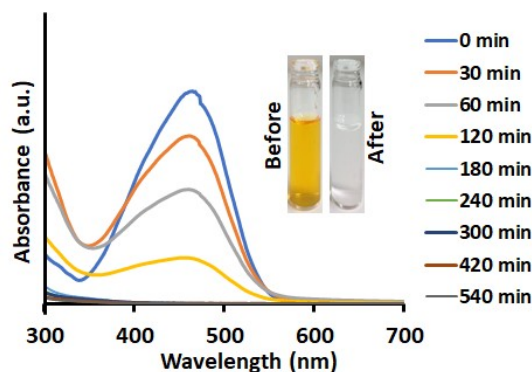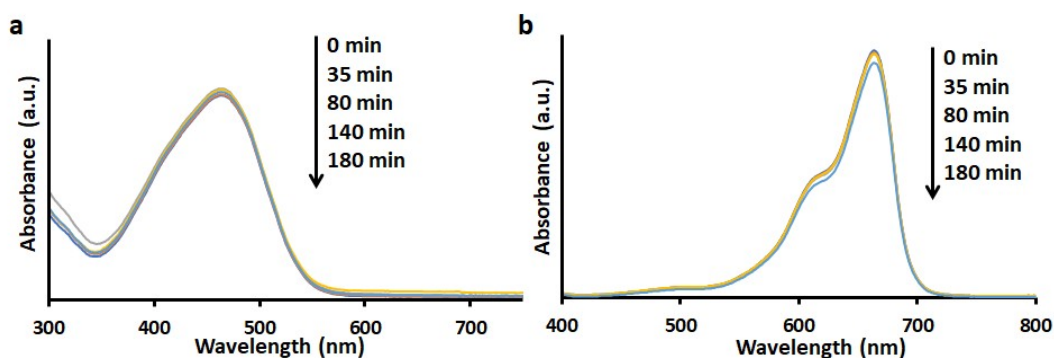
Figure 6. UV visible absorption spectra of initial aqueous solution of MB, supernatant after adsorption of MB on TiO_2-PCHPMA, and the elutant washed out from the TiO_2-PCHPMA adsorbing the MB (concentrations: TiO_2-PCHPMA = 1.5 mg/mL and MB = 10 mg/L, adsorption for 20 min at 28 °C, desorption by washing with MeOH).

3.5. Degradation of Dyes

The photodegradation of MO was conducted under UV irradiation in the presence (Figure 7) and absence (Figure 8a) of TiO_2-PCHPMA. The intensity of the optical absorption of MO in the solution containing TiO_2-PCHPMA decreased with time, and the absorption became unobservable after 180 min. MO was not adsorbed on TiO_2-PCHPMA as previously mentioned, and this result clearly indicates that MO was completely degraded in 180 min. By contrast, MO was not degraded under UV irradiation in the absence of TiO_2-PCHPMA, indicating that the degradation was completely mediated by TiO_2-PCHPMA. The degradation experiment of MO was also conducted in the presence of synthesized TiO_2 under UV irradiation for comparison. The degradation efficiency for MO by TiO_2 was 60% at 1 h, while that by TiO_2-PCHPMA was 65%. The identical efficiencies indicate that the PCHPMA chains in TiO_2-PCHPMA did not affect the diffusion and the degradation of MO due to negligible interaction.
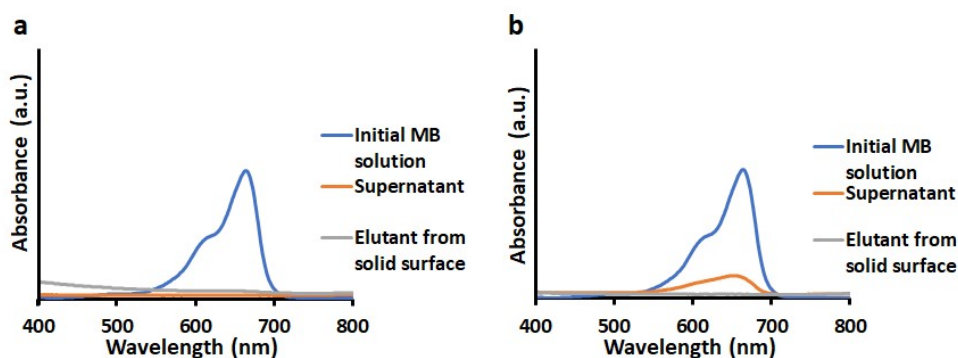

Figure 7. UV-visible absorption spectra of aqueous solution of MO during degradation in the presence of TiO_2-PCHPMA under UV light irradiation with inset photo images of the initial solution of MO and the supernatant after degradation of MO (concentrations: MO = 10 mg/L, TiO_2-PCHPMA = 0.4 mg/mL, 31 °C).

Figure 8. UV-visible absorption spectra of aqueous solution of (**a**) MO and (**b**) MB under UV light irradiation in the absence of TiO_2-PCHPMA for the control experiment (concentrations: MO and MB = 10 mg/L, 31 °C).

The degradation experiment for MB was also carried out in the presence of TiO_2-PCHPMA under UV irradiation (Figure 9a). As a result, MB was degraded in 94% efficiency at 3 h, and the efficiency was higher than that in the presence of bare TiO_2 (80% efficiency) (Figure 9b). However, the residual solid after washing was slightly colored blue, presumably indicating that MB was covalently anchored to the chloroalkyl groups under UV-irradiation, and the degradation efficiency involved slight loss of MB by covalent linkage. The degradation ability of TiO_2-PCHPMA toward MB higher than that of TiO_2 is probably due to the adsorption of cationic MB assisting the approach of MB towards the surface of the TiO_2 core. Acceleration of degradation by adsorption was also reported for TiO_2 modified by polyacrylamide [34], poly [acrylamide-*co*-(acrylic acid)] [40], and NH_4OH [52]. The optical intensity of absorption of MB was not changed in the absence of TiO_2-PCHPMA under UV irradiation in the same manner as MO (Figure 8b), indicating that the degradation of MB was also mediated by TiO_2-PCHPMA.


Figure 9. UV visible absorption spectra of initial aqueous solution of MB, supernatants after degradation of MB by (**a**) TiO_2-PCHPMA and (**b**) TiO_2, and elutants washed out from TiO_2-PCHPMA and TiO_2 after the degradation experiment (concentrations: TiO_2-PCHPMA and TiO_2 = 0.6 mg/mL and MB = 10 mg/L, degradation for 3 h, desorption by washing with MeOH).

3.6. Mechanism of Photocatalysis

The photocatalytic activity of a semiconducting photocatalyst highly depends on the surface modification and the band energy structure. For example, modifications of TiO_2 with silane coupling reagents including MPS decrease the surface modification the photocatalytic activity probably by the blocking of active catalytic sites [64,65]. Figure 10a shows the UV-vis absorption spectrum of PCHPMA. The maximum absorption peak and the onset wavelength appeared at 218 and 244 nm, respectively. These wavelengths are shorter than the wavelengths of the UV emission lines of the Hg lamp (253 and 365 nm). This result indicates that PCHPMA does not contribute to the light absorption.

The band gap calculated from the onset wavelength is 5.1 eV. Figure 10b shows the CV curves of TiO_2-PCHPMA, TiO_2, and PCHPMA in 0.1 M NaCl aq. A peak reduction of TiO_2 was observed from –0.38 V with respect to Ag/AgCl, agreeing well with reported values [8,66,67]. The reduction potential of TiO_2-PCHPMA was observed from -0.28 V with respect to Ag/AgCl, while no peak was observed in the voltammogram of PCHPMA. The small positive shift (+0.1 V) suggests the slightly higher and lowest unoccupied molecular orbital (LUMO) level of TiO_2-PCHPMA due to the change of the chemical structure of the surface of TiO_2, but the effect can be ignored on considering the lower catalytic abilities of reported TiO_2 modified with silane coupling reagents. Accordingly, the primary photocatalytic reaction was not enhanced by the modification. The enhanced degradation occurred by the rapid adsorption of MB on the PCHPMA layer around the surface of TiO_2 in a similar manner to TiO_2 modified by polyacrylamide [34], poly[acrylamide-*co*-(acrylic acid)] [40], and NH_4OH [52]. A plausible mechanism for the degradation of dyes in the presence of TiO_2-PCHPMA under UV irradiation is displayed in Figure 11. The PCHPMA chain grafted on TiO_2 attracts cationic MB to allow the rapid approach of MB over the surface of TiO_2. Adsorbed MB is smoothly degraded by oxidation species such as O_2. By contrast, anionic MO does not interact with the PCHPMA chain, and approaches the surface of TiO_2 by diffusion. As a result, the degradation of MO proceeds identically to TiO_2 and TiO_2-PCHPMA.
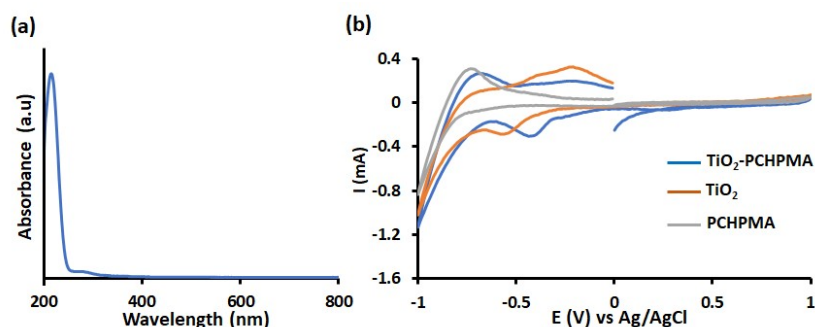
Figure 10. (**a**) UV-vis absorption spectrum of PCHPMA in MeOH and (**b**) cyclic voltammetry (CV) curves of TiO_2-PCHPMA, TiO_2, and PCHPMA deposited on Pt working electrodes (electrolyte, 0.1 M NaCl aq.: counter electrode, Pt wire: reference electrode, Ag wire: sweep rate = 100 mVs^{-1}).
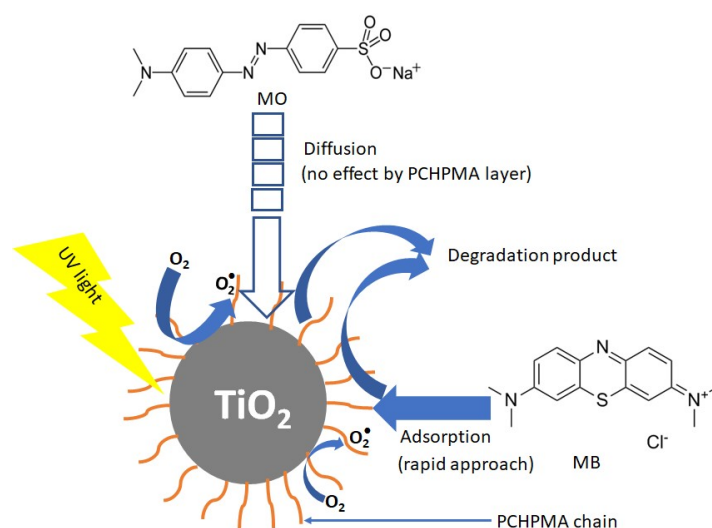
Figure 11. Plausible mechanism for the degradation of dyes in the presence of TiO_2-PCHPMA under UV irradiation.

4. Conclusions

We developed TiO$_2$-PCHPMA for selective separation and degradation of dyes. The structure of TiO$_2$-PCHPMA was confirmed by SEM, TEM, EDX, FTIR, and TGA. The grafted chains of PCHPMA enabled the selective adsorption of cationic MB under a wide pH range from 4 to 12 due to the alkyl chloride group electrostatically interacting with MB, while PCHPMA had no interaction with anionic MO. Adsorbed MB could be either recovered quantitatively by simple washing with methanol or degraded under UV irradiation. The ability of selective adsorption and degradation of TiO$_2$-PCHPMA is beneficial for its potential application to water treatment not only by degradation of pollutants but also by collection for reuse. We are now investigating the effect of TiO$_2$-PCHPMA on various other dyes.

References

1. Robinson, T.; McMulan, G.; Marchant, R.; Nigam, P. Remediation of dyes in textile effluents: A critical review on current treatment technologies with a proposed alternative. *Bioresour. Technol.* **2001**, *77*, 247–255. [CrossRef]

2. Pearce, C.I.; Lioyd, J.R.; Guitrie, J.T. The removal of color from textile wastewater using whole bacterial cells: A review. *Dyes Pigm.* **2003**, *58*, 179–196. [CrossRef]

3. Karan, C.K.; Bhattacharjee, M. Self-healing and moldable metallogels as the recyclable materials for selective dye adsorption and separation. *ACS Appl. Mater. Interfaces* **2016**, *8*, 5526–5535. [CrossRef] [PubMed]

4. Nakata, K.; Fujishima, A. TiO$_2$ photocatalysis: Design and applications. *J. Photochem. Photobiol. C: Photochem. Rev.* **2012**, *13*, 169–189. [CrossRef]

5. Li, H.; Bian, Z.; Zhu, J.; Huo, Y.; Li, H.; Lu, Y. Mesoporous Au/TiO$_2$ nanocomposites with enhanced photocatalytic activity. *J. Am. Chem. Soc.* **2007**, *129*, 4538–4539. [CrossRef] [PubMed]

6. Zhao, D.; Chen, C.; Wang, Y.; Ma, W.; Zhao, J.; Rajh, T.; Zang, L. Enhanced photocatalytic degradation of dye pollutants under visible irradiation on Al(III)-modified TiO$_2$: Structure, interaction, and interfacial electron transfer. *Environ. Sci. Technol.* **2008**, *42*, 308–314. [CrossRef] [PubMed]

7. Naya, S.I.; Nikawa, T.; Kimura, K.; Tada, H. Rapid and complete removal of nonylphenol by gold nanoparticle/rutile titanium(IV) oxide plasmon photocatalyst. *ACS Catal.* **2013**, *3*, 903–907. [CrossRef]

8. Sakthivel, S.; Kisch, H. Daylight photocatalysis by carbon-modified titanium dioxide. *Angew. Chem. Int. Ed.* **2003**, *42*, 4908–4911. [CrossRef] [PubMed]

9. Ren, W.; Ai, Z.; Jia, F.; Zhang, L.; Fan, X.; Zou, Z. Low temperature preparation and visible light photocatalytic activity of mesoporous carbon-doped crystalline TiO$_2$. *Appl. Catal. B* **2007**, *69*, 138–144. [CrossRef]

10. Dong, F.; Guo, S.; Wang, H.; Li, X.; Wu, Z. Enhancement of the visible light photocatalytic activity of c-doped TiO$_2$ nanomaterials prepared by a green synthetic approach. *J. Phys. Chem. C* **2011**, *115*, 13285–13292. [CrossRef]

11. Wang, W.; Serp, P.; Kalck, P.; Faria, J.L. Photocatalytic degradation of phenol on MWNT and titania composite catalysts prepared by a modified sol–gel method. *Appl. Catal. B* **2005**, *56*, 305–312. [CrossRef]

12. Woan, B.K.; Pyrgiotakis, G.; Sigmund, W. Photocatalytic carbon-nanotube–TiO$_2$ composites. *Adv. Mater.* **2009**, *21*, 2233–2239. [CrossRef]

13. Vijayan, B.K.; Dimitrijevic, N.M.; Finkelstein-Shapiro, D.; Wu, J.; Gray, K.A. Coupling titania nanotubes and carbon nanotubes to create photocatalytic nanocomposites. *ACS Catal.* **2012**, *2*, 223–229. [CrossRef]

14. Tryba, B.; Morawski, A.W.; Inagaki, M. Application of TiO$_2$-mounted activated carbon to the removal of phenol from water. *Appl. Catal. B* **2003**, *41*, 427–433. [CrossRef]

15. Asiltürk, M.; Şener, S. TiO₂-activated carbon photocatalysts: Preparation, characterization and photocatalytic activities. *Chem. Eng. J.* **2012**, *180*, 354–363. [CrossRef]

16. Alam, M.G.; Tawfik, A.; Ookawara, S. Enhancement of photocatalytic activity of TiO₂ by immobilization on activated carbon for degradation of pharmaceuticals. *J. Environ. Chem. Eng.* **2016**, *4*, 1929–1937. [CrossRef]

17. Zhang, Y.; Tang, Z.R.; Fu, X.; Xu, Y.J. TiO₂-graphene nanocomposites for gas-phase photocatalytic degradation of volatile aromatic pollutant: Is TiO₂-graphene truly different from other TiO₂-carbon composite materials? *ACS Nano* **2010**, *4*, 7303–7314. [CrossRef] [PubMed]

18. Liang, Y.T.; Vijayan, B.K.; Gray, K.A.; Hersam, M.C. Minimizing graphene defects enhances titania nanocomposite-based photocatalytic reduction of CO₂ for improved solar fuel production. *Nano Lett.* **2011**, *11*, 2865–2870. [CrossRef] [PubMed]

19. Zhao, D.; Sheng, G.; Chen, C.; Wang, X. Enhanced photocatalytic degradation of methylene blue under visible irradiation on graphene@TiO₂ dyade structure. *Appl. Catal. B* **2012**, *111–112*, 302–308. [CrossRef]

20. Liu, B.J.; Bai, H.; Wang, Y.; Liu, Z.; Zhang, X.; Sun, D.D. Self-assembling TiO₂ nanorods on large graphene oxide sheets at a two-phase interface and their anti-recombination in photocatalytic applications. *Adv. Funct. Mater.* **2010**, *20*, 4175–4181. [CrossRef]

21. Sang, Y.; Zhao, Z.; Tian, J.; Hao, P.; Jiang, H.; Liu, H.; Claverie, J.P. Enhanced photocatalytic property of reduced graphene oxide/TiO₂ nanobelt surface heterostructures constructed by an in situ photochemical reduction method. *Small* **2014**, *10*, 3775–3782. [CrossRef] [PubMed]

22. Li, L.; Yu, L.; Lin, Z.; Yang, G. Reduced TiO₂ graphene oxide heterostructure as broad spectrum-driven efficient water-splitting photocatalysts. *ACS Appl. Mater. Interfaces* **2016**, *8*, 8536–8545. [CrossRef] [PubMed]

23. Zhu, Y.; Dan, Y. Photocatalytic activity of poly(3-hexylthiophene)/titanium dioxide composites for degrading methyl orange. *Sol Energy Mater Sol Cells* **2010**, *94*, 1658–1664. [CrossRef]

24. Zhang, H.; Zong, R.; Zhao, J.; Zhu, Y. Dramatic visible photocatalytic degradation performances due to synergetic effect of TiO₂ with PANI. *Environ. Sci. Technol.* **2008**, *42*, 3803–3807. [CrossRef] [PubMed]

25. Min, S.X.; Wang, F.; Feng, L.; Tong, Y.C.; Yang, Z.R. Synthesis and photocatalytic activity of TiO₂/conjugated polymer complex nanoparticles. *Chin. Chem. Lett.* **2008**, *19*, 742–746. [CrossRef]

26. Dimitrijevic, N.M.; Tepavcevic, S.; Liu, Y.; Rajh, T.; Silver, S.C.; Tiede, D.M. Nanostructured TiO₂/polypyrrole for visible light photocatalysis. *J. Phys. Chem. C* **2013**, *117*, 15540–15544. [CrossRef]

27. Gao, F.; Hou, X.; Wang, A.; Chu, G.; Wu, W.; Chen, J.; Zou, H. Preparation of polypyrrole/TiO₂ nanocomposites with enhanced photocatalytic performance. *Particuology* **2016**, *26*, 73–78. [CrossRef]

28. Liao, G.; Chen, S.; Quan, X.; Chen, H.; Zhang, Y. Photonic crystal coupled TiO₂/polymer hybrid for efficient photocatalysis under visible light irradiation. *Environ. Sci. Technol.* **2010**, *44*, 3481–3485. [CrossRef] [PubMed]

29. Luo, Q.; Li, X.; Li, X.; Wang, D.; An, J.; Li, X. Visible light photocatalytic activity of TiO₂ nanoparticles modified by pre-oxidized polyacrylonitrile. *Catal. Commun.* **2012**, *26*, 239–243. [CrossRef]

30. Wang, D.; Zhang, J.; Luo, Q.; Li, X.; Duan, Y.; An, J. Characterization and photocatalytic activity of poly(3-hexylthiophene)-modified TiO₂ for degradation of methyl orange under visible light. *J. Hazard. Mater.* **2009**, *169*, 546–550. [CrossRef] [PubMed]

31. Mahanta, D.; Manna, U.; Madras, G.; Patil, S. Multilayer self-assembly of TiO₂ nanoparticles and polyaniline-grafted-chitosan copolymer (CPANI) for photocatalysis. *ACS Appl. Mater. Inter.* **2011**, *3*, 84–92. [CrossRef] [PubMed]

32. Li, X.; Wang, D.; Cheng, G.; Luo, Q.; An, J.; Wang, Y. Preparation of polyaniline-modified TiO₂ nanoparticles and their photocatalytic activity under visible light illumination. *Appl. Catal. B* **2008**, *81*, 267–273. [CrossRef]

33. Wang, D.; Wang, Y.; Li, X.; Luo, Q.; An, J.; Yue, J. Sunlight photocatalytic activity of polypyrrole–TiO₂ nanocomposites prepared by 'in situ' method. *Catal. Commun.* **2008**, *9*, 1162–1166. [CrossRef]

34. Tang, Q.; Lin, J.; Wu, Z.; Wu, J.; Huang, M.; Yang, Y. Preparation and photocatalytic degradability of TiO₂/polyacrylamide composite. *Eur. Polym. J.* **2007**, *43*, 2214–2220. [CrossRef]

35. Yang, C.; Zhang, M.; Dong, W.; Cui, G.; Ren, Z.; Wang, W. Highly efficient photocatalytic degradation of methylene blue by PoPD/TiO₂ nanocomposite. *PLoS ONE* **2017**, *12*, e0174104. [CrossRef] [PubMed]

36. Wang, F.; Min, S.; Han, Y.; Feng, L. Visible-light-induced photocatalytic degradation of methylene blue with polyaniline-sensitized TiO₂ composite photocatalysts. *Supperlatt. Microstruct.* **2010**, *48*, 170–180. [CrossRef]

37. Xu, S.; Gu, L.; Wu, K.; Yang, H.; Song, Y.; Jiang, L.; Dan, Y. The influence of the oxidation degree of poly(3-hexylthiophene) on the photocatalytic activity of poly(3-hexylthiophene)/TiO₂ composites. *Sol. Energy Mater. Sol. Cells.* **2012**, *96*, 286–291. [CrossRef]

38. Luo, Q.; Wang, X.; Wang, D.; An, J.; Li, X.; Yin, R. TiO$_2$/cyclized polyacrylonitrile hybridized nanocomposite: An efficient visible-light photocatalyst prepared by a facile "in situ" approach. *Mater. Sci. Eng. B* **2015**, *199*, 96–104. [CrossRef]

39. Muthirulan, P.; Nirmala, C.K.; Sundaram, M.M. Facile synthesis of novel hierarchical TiO$_2$@Poly(o-phenylenediamine) core–shell structures with enhanced photocatalytic performance under solar light. *J. Environ. Chem. Eng.* **2013**, *1*, 620–627. [CrossRef]

40. Kangwansupamonkon, W.; Jitbunpot, W.; Kiatkamjornwong, S. Photocatalytic efficiency of TiO$_2$/poly[acrylamide-co-(acrylic acid)] composite for textile dye degradation. *Polym. Degrad. Stabil.* **2010**, *95*, 1894–1902. [CrossRef]

41. Fukahori, S.; Ichiura, H.; Kitaoka, T.; Tanaka, H. Photocatalytic decomposition of bisphenol A in water using composite TiO$_2$-zeolite sheets prepared by a papermaking technique. *Environ. Sci. Technol.* **2003**, *37*, 1048–1051. [CrossRef] [PubMed]

42. Liu, B.; Wen, L.; Nakata, K.; Zhao, X.; Liu, S.; Ochiai, T.; Murakami, T.; Fujishima, A. Polymeric adsorption of methylene blue in TiO$_2$ colloids-highly sensitive thermochromism and selective photocatalysis. *Chem. Eur. J.* **2012**, *18*, 12705–12711. [CrossRef] [PubMed]

43. Zang, G.; Choi, W.; Kim, S.H.; Hong, S.B. Selective photocatacatalytic degradation of aquatic pollutants by titania encapsulated into FAU-type zeolites. *J. Hazard. Mater.* **2011**, *188*, 198–205. [CrossRef] [PubMed]

44. Shen, X.; Zhu, L.; Liu, G.; Yu, H.; Tang, H. Enhanced photocatalytic degradation and selective removal of nitrophenol by using surface molecular imprinted titania. *Environ. Sci. Technol.* **2008**, *42*, 1687–1692. [CrossRef] [PubMed]

45. Inumaru, K.; Murashima, M.; Kasahara, T.; Yamanaka, S. Enhanced photocatalytic decomposition of 4-nonylphenol by surface-organografted TiO$_2$: a combination of molecular selective adsorption and photocatalysis. *Appl. Catal. B* **2004**, *52*, 275–280. [CrossRef]

46. Nakamura, K.J.; Ide, Y.; Ogawa, M. Molecular recognitive photocatalytic decomposition on mesoporous silica coated TiO$_2$ particle. *Mater. Lett.* **2011**, *65*, 24–26. [CrossRef]

47. Bao, L.; Meng, M.; Sun, K.; Li, W.; Zhao, D.; Li, H.; He, M. Selective adsorption and degradation of rhodamine B with modified titanium dioxide photocatalyst. *J. Appl. Polym. Sci.* **2014**, *40890*, 1–12. [CrossRef]

48. Choi, H.; Kim, Y.J.; Varma, R.S.; Dionysiou, D.D. Thermally stable nanocrystalline TiO$_2$ photocatalysts synthesized via sol-gel methods modified with ionic liquid and surfactant molecules. *Chem. Mater.* **2006**, *18*, 5377–5384. [CrossRef]

49. Kumar, S.G.; Devi, L.G. Review on modified TiO$_2$ photocatalysis under UV/visible light: selected results and related mechanisms on interfacial charge carrier transfer dynamics. *J. Phys. Chem. A* **2011**, *115*, 13211–13241. [CrossRef] [PubMed]

50. Lazar, M.A.; Walid, A.; Daoud, W.A. Achieving selectivity in TiO$_2$-based photocatalysis. *RSC Adv.* **2013**, *3*, 4130–4140. [CrossRef]

51. Robert, D.; Piscopo, A.; Weber, J.V. First approach of the selective treatment of water by heterogeneous photocatalysis. *Environ. Chem. Lett.* **2004**, *2*, 5–8. [CrossRef]

52. Lazar, M.A.; Daoud, W.A. Selective adsorption and photocatalysis of low-temperature base-modified anatase nanocrystals. *RSC Adv.* **2012**, *2*, 447–452. [CrossRef]

53. Genevrier, A.C.; Boissiere, C.; Nicole, L.; Grosso, D. Distance dependence of the photocatalytic efficiency of TiO$_2$ revealed by in situ ellipsometry. *J. Am. Chem. Soc.* **2012**, *134*, 10761–10764. [CrossRef] [PubMed]

54. Gokaltun, A.; Çelebi, B.; Tuncel, A. Octadecylamine-attached poly(3-chloro-2-hydroxypropyl methacrylate-*co*-ethylene dimethacrylate) microspheres as a new stationary phase for microbore reversed phase chromatography. *Anal. Meth.* **2014**, *6*, 5712–5719. [CrossRef]

55. Molina, E.A.; Néstor, R.V.; Rodríguez, D.M.; Figueiras, C.C. Synthesis and characterization of TiO$_2$ modified with polystyrene and poly(3-chloro-2hydroxypropyl methacrylate) as adsorbents for the solid phase extraction of organophosphorous pesticides. *J. Chem.* **2016**, *2016*, 1–11. [CrossRef]

56. Cozzoli, P.D.; Kornowski, A.; Weller, H. Low-temperature synthesis of soluble and processable organic-capped anatase TiO$_2$ nanorods. *J. Am. Chem. Soc.* **2003**, *125*, 14539–14548. [CrossRef] [PubMed]

57. Wang, C.; Mao, H.; Wang, C.; Fu, S. Dispersibility and hydrophobicity analysis of titanium dioxide nanoparticles grafted with silane coupling agent. *J. Ind. Eng. Chem. Res.* **2011**, *50*, 11930–11934. [CrossRef]

58. Yuvaraj, H.; Kim, W.S.; Kim, J.T.; Kang, I.P.; Gal, Y.S.; Kim, S.W.; Lim, K.T. Synthesis of poly(methyl methacrylate) encapsulated TiO_2 nanocomposite particles in supercritical CO_2. *Mol. Cryst. Liq. Cryst.* **2009**, *514*, 355–365. [CrossRef]

59. Wang, J.; Sun, W.; Zhang, Z.; Jiang, Z.; Wang, X.; Xu, R.; Li, R.; Zhang, X. Preparation of Fe-doped mixed crystal TiO_2 catalyst and investigation of its sonocatalytic activity during degradation of azo fuchsine under ultrasonic irradiation. *J. Colloid Interface Sci.* **2008**, *320*, 202–209. [CrossRef] [PubMed]

60. Sun, X.; Liu, H.; Dong, J.; Wei, J.; Zhang, Y. Preparation and Characterization of Ce/N-Codoped TiO_2 Particles for Production of H_2 by Photocatalytic Splitting Water Under Visible Light. *Catal. Lett.* **2010**, *135*, 219–225. [CrossRef]

61. Ba-abbad, M.M.; Kadhum, A.A.H.; Mohamad, A.B.; Takriff, M.S.; Sopian, K. Synthesis and catalytic activity of TiO_2 nanoparticles for photochemical oxidation of concentrated chlorophenols under direct solar radiation. *Int. J. Electrochem. Sci.* **2012**, *7*, 4871–4888.

62. Wang, Y.Q.; Chen, S.G.; Tang, X.H.; Palchik, O.; Zaban, A.; Koltypin, Y.; Gedanken, A. Mesoporous titanium dioxide: sonochemical synthesis and application in dye-sensitized solar cells. *J. Mater. Chem.* **2001**, *11*, 521–526. [CrossRef]

63. Yu, J.C.; Zhang, L.; Yu, J. Direct sonochemical preparation and characterization of highly active mesoporous TiO_2 with a bicrystalline framework. *Chem. Mater.* **2002**, *14*, 4647–4653. [CrossRef]

64. Pazokifard, S.; Mirabedini, S.M.; Esfandeh, M.; Mohseni, M.; Ranjbar, Z. Silane grafting of TiO_2 nanoparticles: dispersibility and photoactivity in aqueous solutions. *Surf. Interface Anal.* **2012**, *44*, 41–47. [CrossRef]

65. Siddiquey, I.A.; Ukaji, E.; Furusawa, T.; Sato, M.; Suzuki, N. The effects of organic surface treatment by methacryloxypropyltrimethoxysilane on the photostability of TiO_2. *Mater. Chem. Phys.* **2007**, *105*, 162–168. [CrossRef]

66. Pelouchova, H.; Janda, P.; Weber, J.; Kavan, L. Charge transfer reductive doping of single crystal TiO_2 anatase. *J. Electro. Chem.* **2004**, *566*, 73–83. [CrossRef]

67. Renault, C.; Nicole, L.; Sanchez, C.; Costentin, C.; Balland, V.; Limoges, B. Unraveling the charge transfer/electron transport in mesoporous semiconductive TiO_2 films by voltabsorptometry. *Phys. Chem. Chem. Phys.* **2015**, *17*, 10592–10607. [CrossRef] [PubMed]